

Supplementary Information

Sensing array of radically coupled genetic biopixels

Arthur Prindle,^{1*} Phillip Samayoa,^{2*} Ivan Razinkov,¹ Tal Danino,¹ Lev S. Tsimring,³
and Jeff Hasty^{1,2,3,4,5}

November 8, 2011

¹ *Department of Bioengineering, University of California, San Diego, San Diego, California, USA.*

² *Bioinformatics Program, University of California, San Diego, La Jolla, California, USA.*

³ *BioCircuits Institute, University of California, San Diego, San Diego, California, USA.*

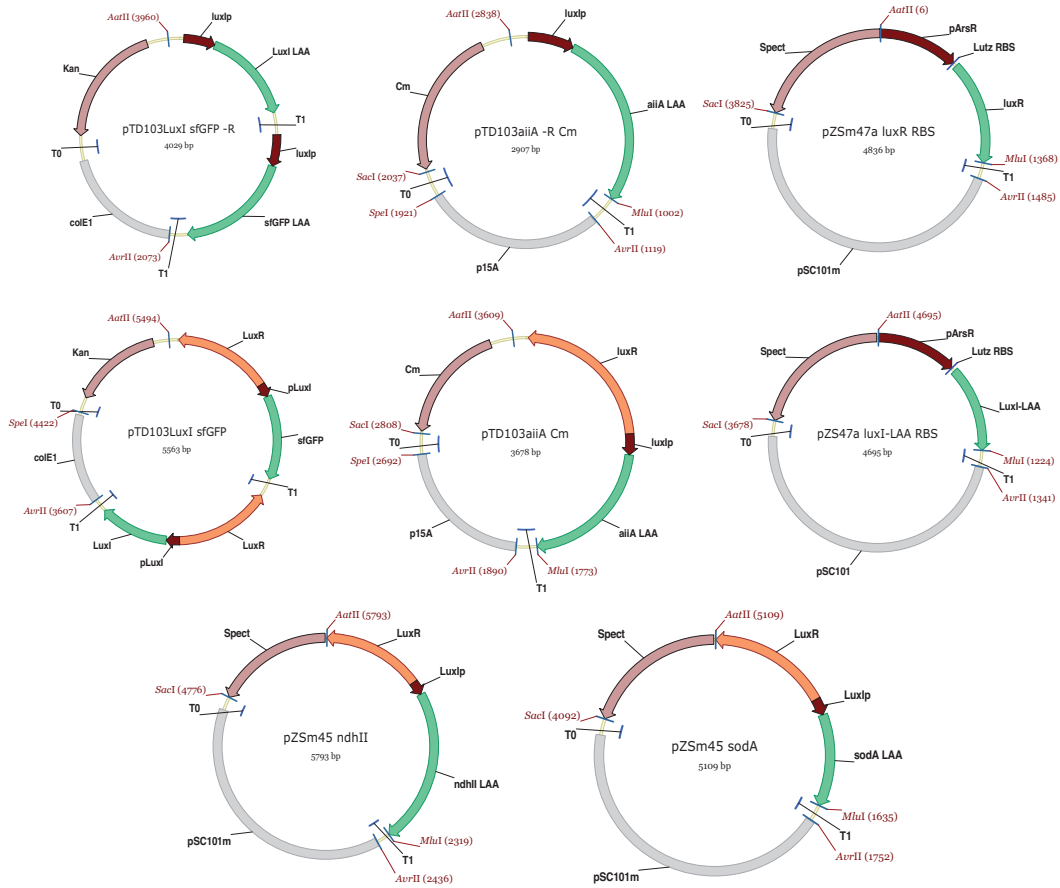
⁴ *Molecular Biology Section, Division of Biological Science, University of California, San Diego, La Jolla, CA 92093, USA*

⁵ *Corresponding Author. Molecular Biology Section, Division of Biological Science, University of California, San Diego, Mailcode 0412, La Jolla, CA 92093-0412, USA. Telephone: 858 822 3442. Fax: 858 534 5722. Email: hasty@ucsd.edu*

* These authors contributed equally to this work.

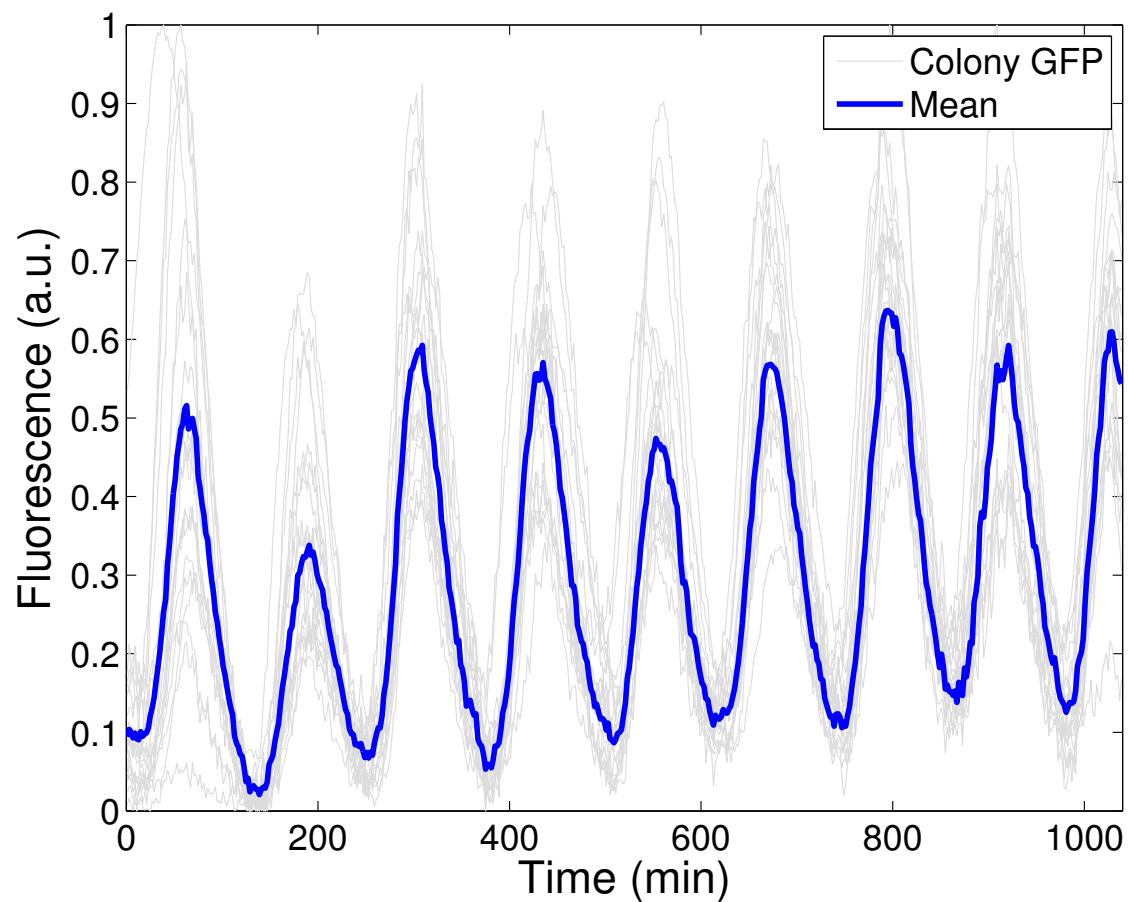
Plasmid Construction

The oscillator plasmids were constructed by modifying the constructs used in a previous study (1). The antibiotic resistance genes of pTD103AiiA was switched to chloramphenicol. The reporter protein on pTD103LuxI/GFP was switched to a recently reported superfolding green fluorescent protein, sfGFP (2). The *ndh* and *sodA* genes were amplified directly from the native *E. coli* genome by PCR. Promoter output was tuned by changing the RBS sequence and quantified using flow cytometry. We initially constructed the sensing plasmid with a published synthetic background-reduced version that contains additional ArsR operator sites(3) but failed to produce enough LuxR. To increase LuxR output, we reverted to the native promoter sequence, switched the RBS to that of pZ plasmids(?), and increased the copy number by a factor of 5 by switching to a mutated SC101 origin of replication. All circuit components except LuxR were tagged by PCR with a carboxy-terminal *ssrA* tag (AANDENYALAA) (4) for fast degradation. Modular pieces (resistance genes, promoters, origins, and ORFs) were assembled using a PCR-based cloning scheme named CPEC (5).

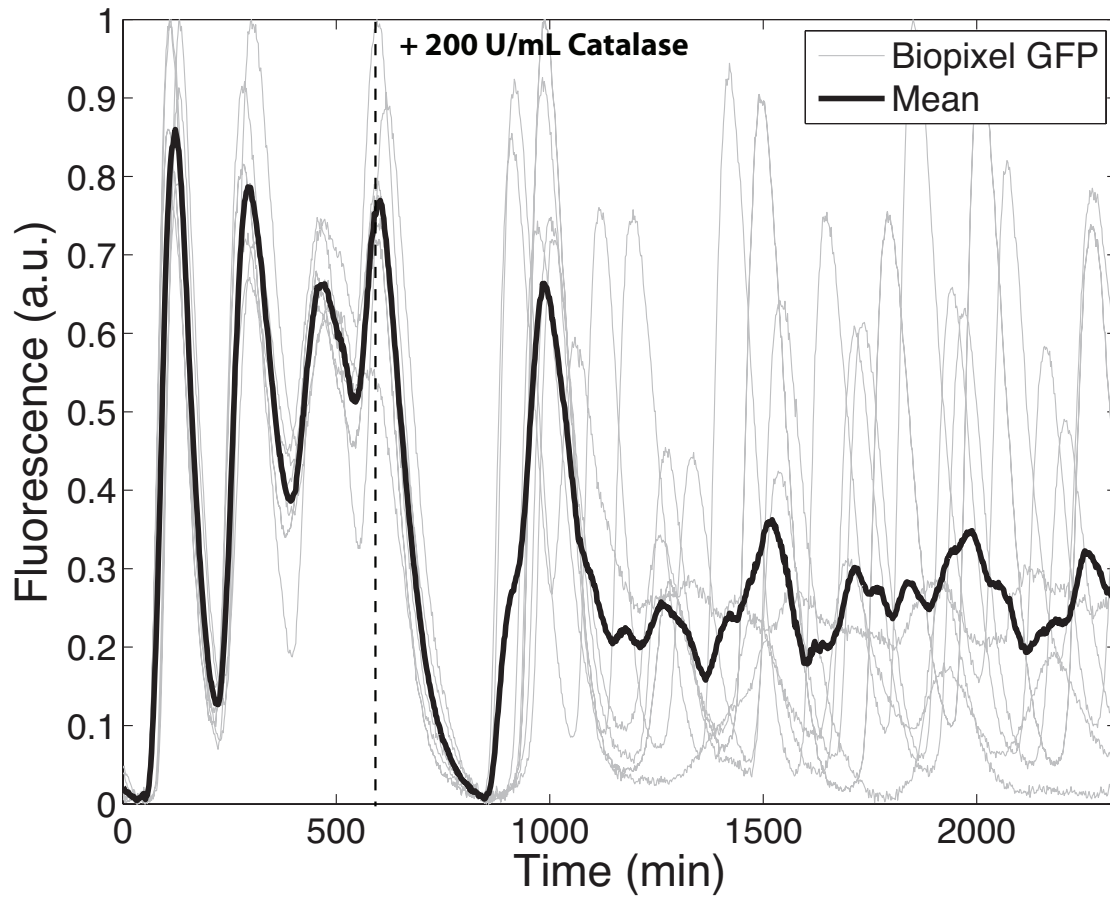


Supplementary Figure 1: Plasmids used in this study. Top row is the thresholding sensor: 2 oscillator plasmids with *luxR* genes removed and a plasmid containing *pArs::luxR*. Middle row is the period modulator: 2 oscillator plasmids and a plasmid containing *pArs::luxI-laa*. Bottom row contains 2 plasmids used to study H_2O_2 production and synchronization: *pLux::ndh* and *pLux::sodA*. NDH-2 synchronization strain is the oscillator plasmids with *pZSm45 ndhII*.

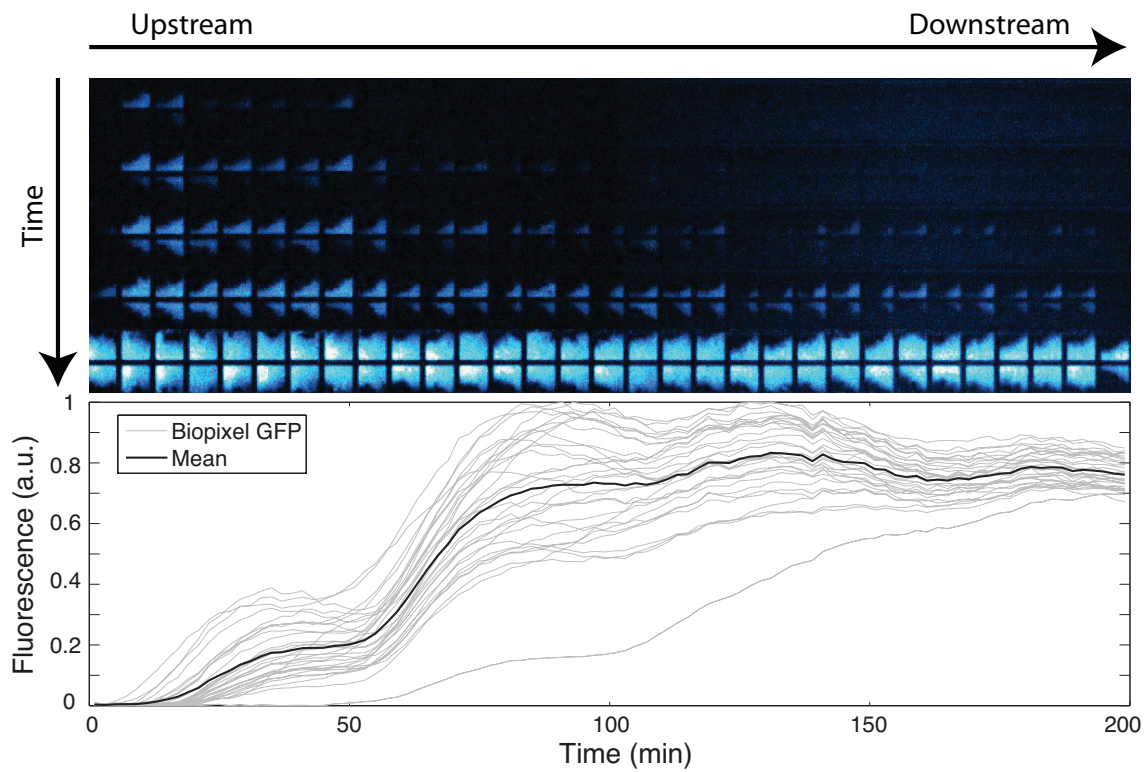
Additional Experimental Results



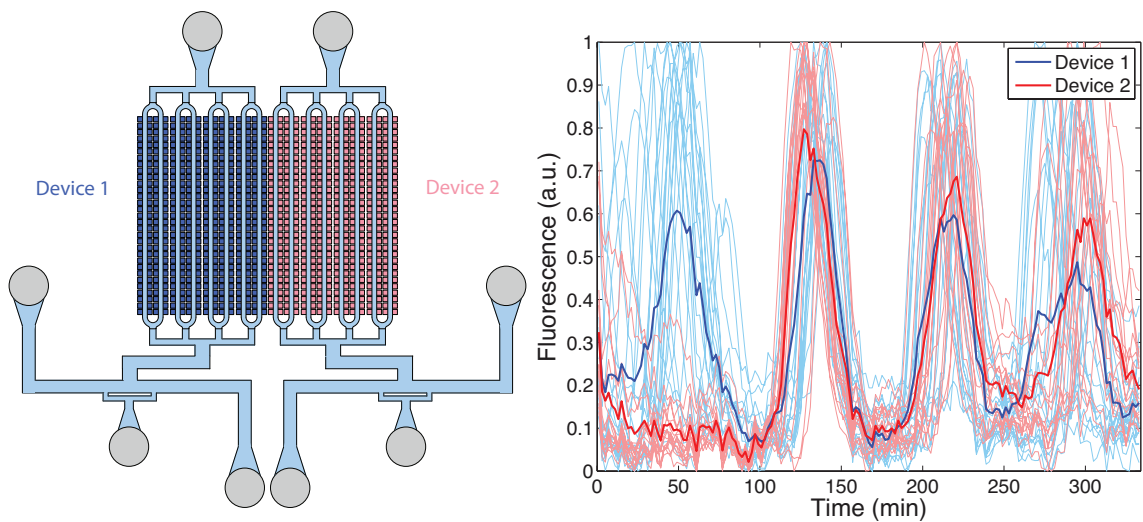
Supplementary Figure 2: Biopixels with NDH-2 engineered synchronization observed at ultra-low fluorescence (4X, 20ms exposure, 3% power) using an EMCCD camera to ensure no fluorescence interaction. Synchronized oscillations are maintained across the array for the length of the experiment (14 hours).



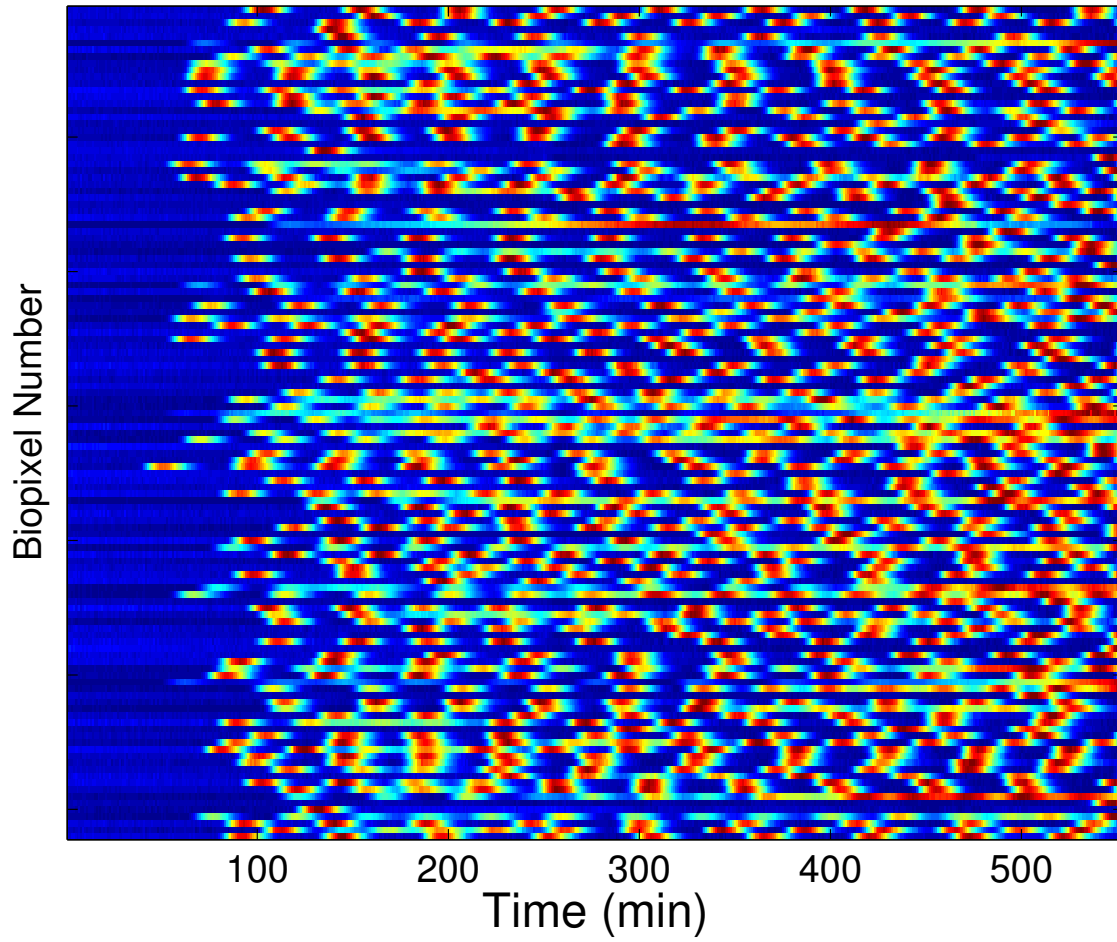
Supplementary Figure 3: Catalase degrades external H_2O_2 and prevents communication between colonies. When a synchronized population of biopixels was exposed to a step increase of 200 U/ml catalase, synchronization was broken and biopixels continued to oscillate individually. Since catalase can't cross the cell membrane, this shows that synchronization between colonies depends on H_2O_2 but oscillations with a colony do not.



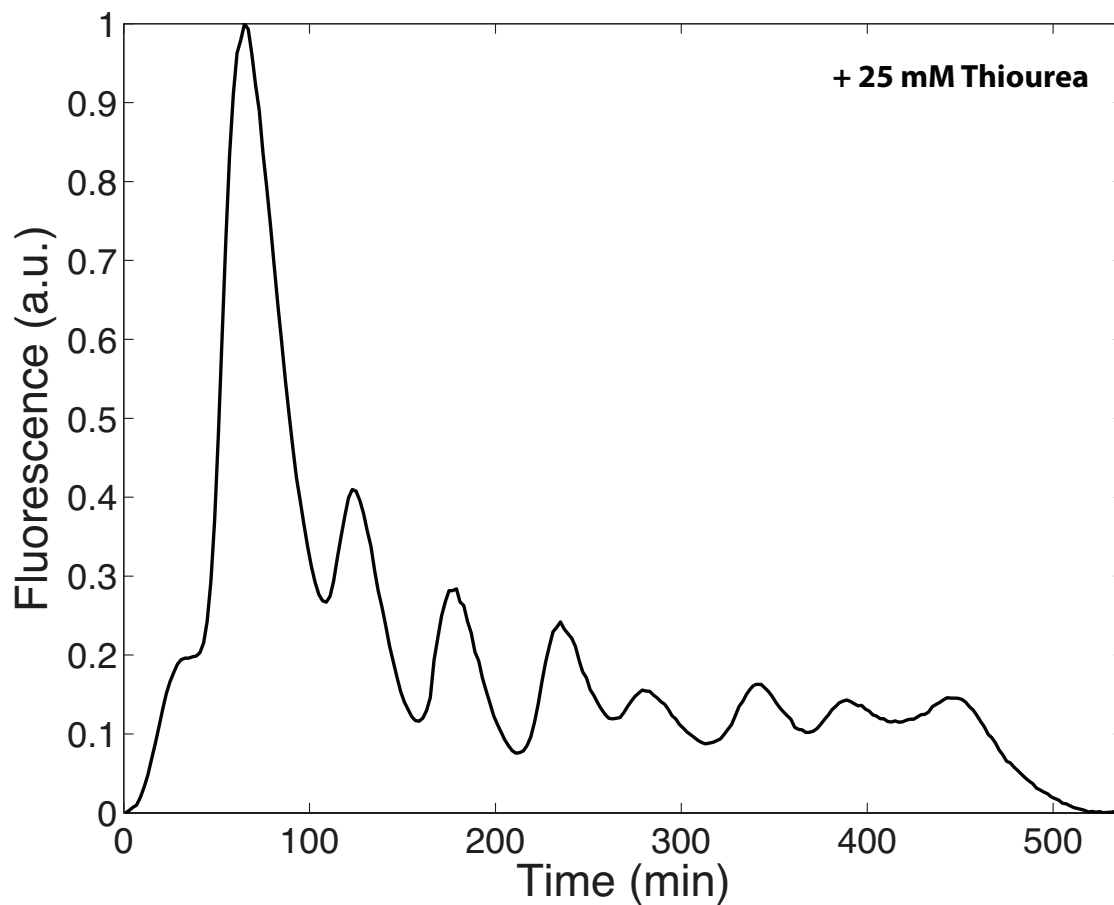
Supplementary Figure 4: SodA produces H_2O_2 internal to the cell, permanently switching the cellular redox state (oxidizing) thereby activating lux-controlled genes. Biopixels rapidly fire and lock on in a spatial wave, far earlier than is typical for colonies of this size. The propagation of ON biopixels suggests that colonies are capable of activating those nearby via migrating H_2O_2 species.



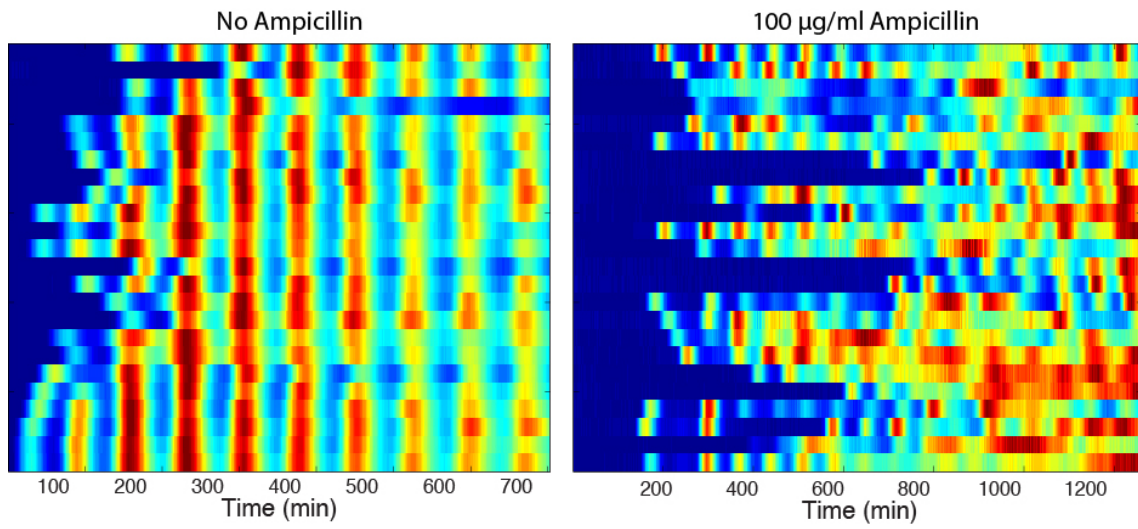
Supplementary Figure 5: Synchronized oscillations occur across 2 fluidically isolated devices held in close proximity. In this experiment, the devices were started at different times yet become synchronized. Since these devices share no common fluid sources or sinks, this confirms that synchronization is mediated by vapor species.



Supplementary Figure 6: Heatmap of trajectories extracted from low fluorescence intensity control (Suppl. Movie 9) when NDH-2 plasmid is not present. Biopixels oscillate individually but fail to synchronize.



Supplementary Figure 7: The introduction thiourea, a potent radical quencher, produces decaying synchronized oscillations across a population of biopixels. Because radical species are precursors for H_2O_2 , eliminating them lowers the production of H_2O_2 and therefore dampens the oscillations. Colonies are still able to synchronize because, while thiourea eliminates radicals within cells, it does not prevent H_2O_2 from diffusing between cells.



Supplementary Figure 8: Synchronization is prevented when 100 µg/ml Ampicillin is used in the media. The constructs, strains, and experimental conditions are otherwise identical.

Data Analysis

Fluorescence data was obtained by importing fluorescent images into ImageJ and subtracting cell signal from background signal. Oscillatory period was taken to be the average of peak-to-peak and trough-to-trough distance, calculated using a MATLAB script. The data represented in Fig. 1d and 2b-d were collected by stitching 4 images taken at 4X magnification. The mean trajectory in Fig. 1d was found by averaging 373 individual biopixel trajectories, of which 20 are shown. Biopixel trajectories were extracted from image series using a MATLAB script, where a bright field image of the corresponding array was used to generate a mask. The data shown in Fig. 2c was measured over 4 separate experiments using 10-30 oscillatory periods per data point.

Sensor calibration curve (Fig. 2c, bottom) was generated using a series of 2-population ttests comparing the experimental datasets to randomly generated new sample sets. The mean of generated sets was decremented until the ttest failed with $\alpha = 95\%$, indicating the lowest period that could be associated with that arsenite concentration. We repeated this process for each arsenite level and fit the points with a quadratic since we expected it to take the inverse shape of the period vs. arsenite measurements.

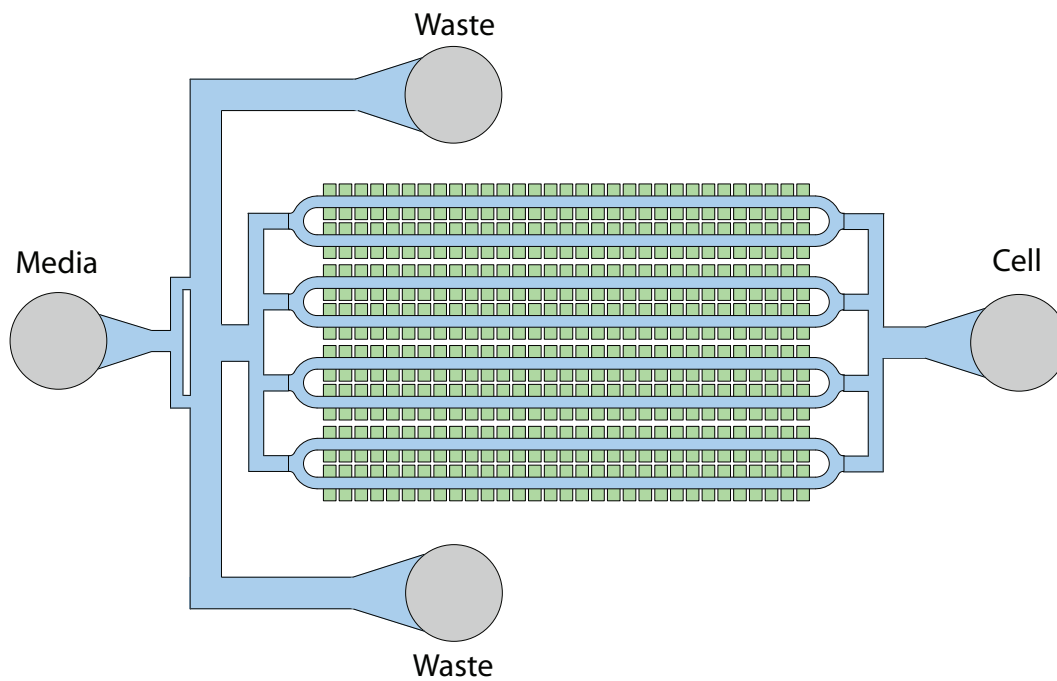
Microscopy and Microfluidics

We used a microscopy system similar to our recent studies (1), with the addition of a high-sensitivity Andor DU-897 EMCCD camera. Fluorescent images were taken at 4X every 30 seconds using the EMCCD camera (20ms exposure, 97% attenuation) or 2 minutes (2s exposure, 90% attenuation) using a standard CCD camera to prevent photobleaching or phototoxicity.

In each device, *E. coli* cells are loaded from the cell port while keeping the media port at sufficiently higher pressure than the waste port below to prevent contamination (Suppl. Fig 8). Cells were loaded into the cell traps by manually applying pressure pulses to the lines to induce a momentary flow change. The flow was then reversed and allowed for cells to receive fresh media with 0.075% Tween which prevented cells from adhering to the main channels and waste ports.

To measure fluid flow rate before each experiment, we measured the streak length of fluorescent beads ($1.0 \mu\text{m}$) upon 100 ms exposure to fluorescent light. We averaged at least 1,000 data points for each.

We constructed several microfluidic devices over the course of the study. The trap dimensions were always $100 \mu\text{m} \times 85 \mu\text{m} \times 1.65 \mu\text{m}$ high, which we previously found to be optimal for oscillator function, except when size was varied to study dynamic interactions. Spacing between traps was $25 \mu\text{m}$, except in devices designed to study the effects of increasing separation distance between traps. For sensor array devices, we constructed 500 and 12,000 trap arrays as well as a tandem device which holds two 150 trap arrays in close proximity ($25 \mu\text{m}$) without sharing fluid sources or sinks.



Supplementary Figure 9: Primary microfluidic device used for this study. Media containing variable arsenite concentration is fed through the cell port, flowing past the biopixel array into the cell and waste ports. During loading, pressure is increased at the cell port and decreased at the waste ports to reverse the flow, allowing cells to pass by the trapping regions. Other microfluidic devices used have the same layout with trap number, separation, and size varied.

Modeling

To model the dynamics of the quorum-sensing oscillator, we used our previously described model for intracellular concentrations of LuxI (I), AiiA (A), internal AHL (H_i), and external AHL (H_e) (1),

$$\frac{\partial A}{\partial t} = C_A[1 - (d/d_0)^4] G(\alpha, \tau) - \frac{\gamma_A A}{1 + f(A + I)} \quad (1)$$

$$\frac{\partial I}{\partial t} = C_I[1 - (d/d_0)^4] G(\alpha, \tau) - \frac{\gamma_I I}{1 + f(A + I)} \quad (2)$$

$$\frac{\partial H_i}{\partial t} = \frac{bI}{1 + kI} - \frac{\gamma_H A H_i}{1 + gA} + D(H_e - H_i) \quad (3)$$

$$\frac{\partial H_e}{\partial t} = -\frac{d}{1-d} D(H_e - H_i) - \mu H_e + D_1 \frac{\partial^2 H_e}{\partial x^2} \quad (4)$$

In the original model, the concentration of the constitutively produced LuxR protein R was assumed constant. In the ON/OFF threshold arsenic biosensor circuit, LuxR production is induced by arsenic, which we model by the equation

$$\dot{R} = \frac{\alpha_c A}{(A_0 + A)} - \gamma_R R \quad (5)$$

in which the LuxR expression from the arsenic promoter follows a standard saturating function of the arsenic concentration A . Accordingly, we modified the Hill function for Lux promoter to include the explicit dependence on R :

$$G(\alpha, \tau) = \frac{\delta + \alpha (R_\tau H_\tau)^2}{1 + k_1 (R_\tau H_\tau)^2} \quad (6)$$

For modeling the period-modulating sensor, we modified the equation for LuxI (2) to include additional production from the arsenic promoter,

$$\dot{I} = C_I[1 - (d/d_0)^4] G(\alpha, \tau) + \frac{\alpha_c A}{(A_0 + A)} - \frac{\gamma_I I}{1 + f(A + I)} \quad (7)$$

The following additional parameters were used for the biosensor simulations: $\alpha_c = 50$, $A_0 = 2$, $\gamma_R = .1$.

Arsenic levels were swept across the dynamic range of the arsenic promoter to produce the curve in Fig. 2c. The period for each arsenic level was calculated from the peak-to-peak average of 15 oscillatory periods.

To model the spatial synchronization of oscillating colonies across a microfluidic array, we generalized a simplified "degrade-and-fire" model (6). The delay-differential equation

$$\dot{X}_{i,j} = \frac{\alpha(1 + vP_{i,j,\tau_2})}{(1 + \frac{X_{i,j,\tau_1}}{C_0})^2} - \frac{\gamma X_{i,j}}{k + X_{i,j}} \quad (8)$$

describes oscillations of individual biopixel $\{i, j\}$ as a combined effect of production and delayed autorepression (first term in the r.h.s.) of the colony-averaged LuxI concentration $X_{i,j}$ and its enzymatic degradation by ClpXP (second term). Unlike (6), the first (production) term in Eq. 8 describes both delayed auto-repression of LuxI and its delayed activation by H_2O_2 proportional to its local concentration $P_{i,j}$. Subscripts τ_1 and τ_2 indicate the delayed concentrations, $X_{i,j,\tau_1}(t) = X_{i,j}(t - \tau_1)$ and $P_{i,j,\tau_2}(t) = P_{i,j}(t - \tau_2)$. The dynamics of $P_{i,j}$ is described by the equation

$$\dot{P}_{i,j} = \mu + \alpha_p X_{i,j} - \gamma_p P_{i,j} + \hat{S}\{P_{i,j}\} \quad (9)$$

where the first three terms describe the basal and induced production and degradation of H_2O_2 . The last term models the spatial coupling of neighboring biopixels via the H_2O_2 exchange. For a square $N \times N$ array of traps, we used the following discrete diffusion form of the spatial operator,

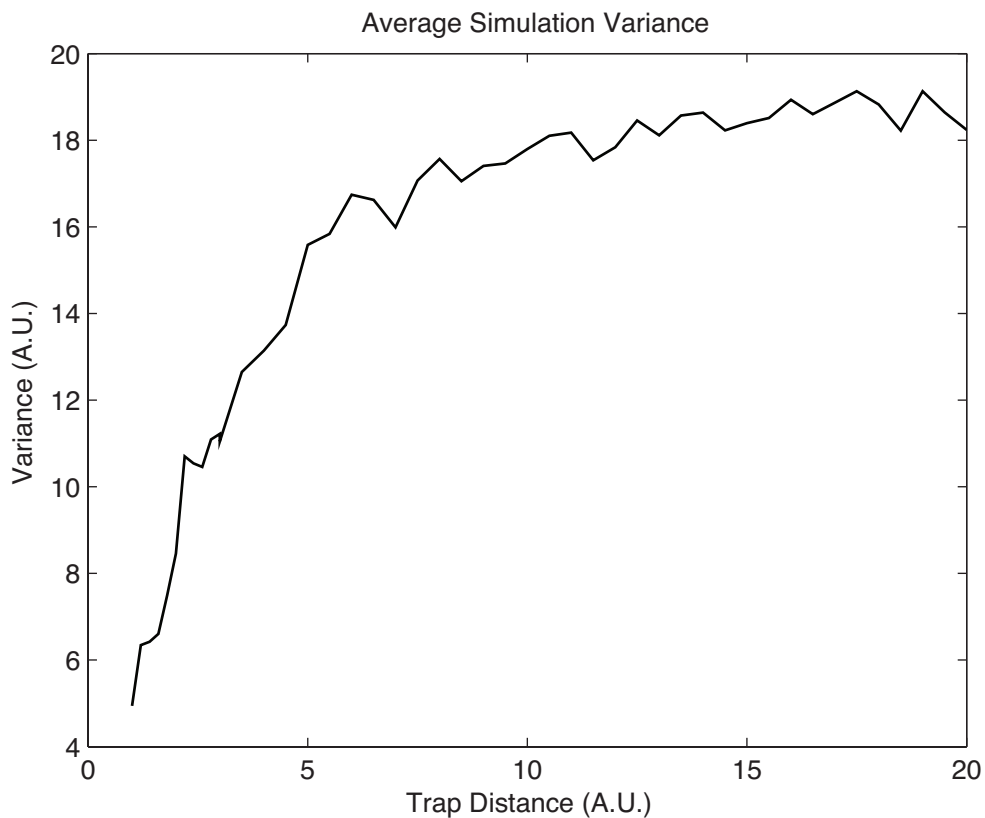
$$\hat{S}\{P_{i,j}\} = D\Delta^{-2}[P_{i-1,j} + P_{i+1,j} + P_{i,j-1} + P_{i,j+1} - 4P_{i,j}] \quad (10)$$

Each colony is affected by the H_2O_2 produced in four neighboring colonies, two in each dimension of the array, separated by the equal distance Δ . We used the boundary condition $P_{i,j} = 0$ for the edges of the array $i, j = 0, N + 1$. This represents the infinite external sink of H_2O_2 diffusing out of the microfluidic chip. The diffusion operator above can be generalized if the row spacing differs from the column spacing, or for other spatial arrangements of colonies within the biosensor.

We introduced variability among different traps by randomizing oscillator parameters for individual traps in each simulation. Specifically, LuxI (X) activation and degradation parameters ($p = \{\alpha, \gamma\}$) of each of the oscillators in the array were varied around their nominal values (p_0) as $p = p_0 + \delta$ where δ is a random number uniformly distributed between -0.25 and 0.25 . We used the following dimensionless parameters for most of our simulations: $\alpha_0 = 8.25$, $\gamma_0 = 5.75$, $\nu = 1$, $\tau_1 = 10$, $\tau_2 = 20$, $C_0 = 6$, $k = 10$, $\mu = 20$, $\alpha_p = 1$, $\gamma_p = 10$, $D = 7$, $\Delta = 1$.

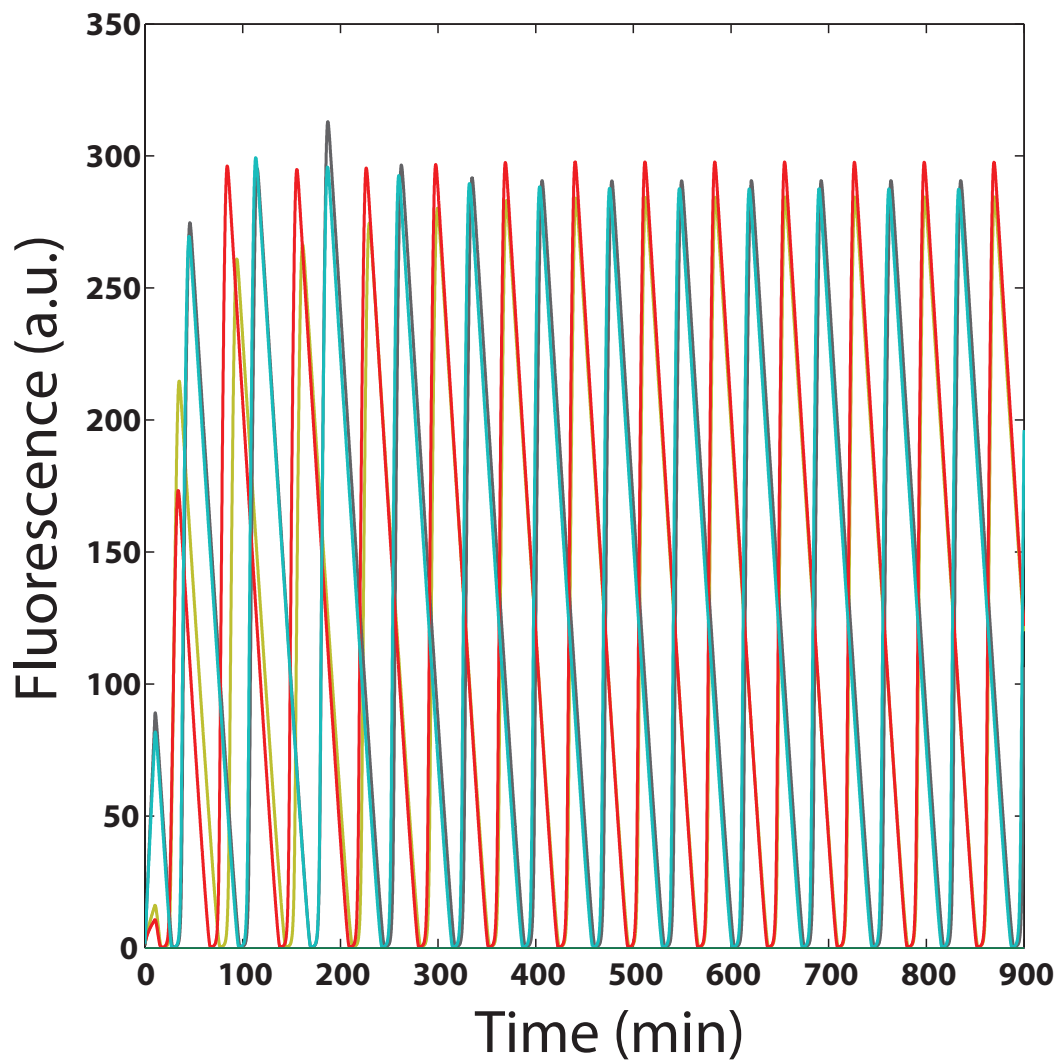
For the characterization of various regimes of array synchronization, 16 colonies were modeled in the 4×4 array. Scaling up the simulation with larger numbers of colonies produced equivalent results. Overproduction of H_2O_2 by expressing *sodA* was captured by increasing α_p 20-fold. This is consistent with expression from a pSC101m plasmid with a copy number of 20-30. Depletion of external H_2O_2 by catalase was modeled by increasing H_2O_2 degradation (γ_p) and decreasing H_2O_2 diffusion, D . In Suppl. Fig. 9 we show the variance of the concentrations $X_{i,j}$ within the array averaged over time and parameter variations. This plot demonstrates that the synchronicity among the biopixels decreases with increase of spacing among them, and for $\Delta > 5$ is completely lost.

Increasing the trap spacing Δ 2-fold while simultaneously decreasing k 4-fold allowed us to reproduce the more complex waveforms observed experimentally in our arrays. Note that changing k models the change of the trap depth. As the size of the trap decreases, the flow of media is able to more rapidly sweep away AHL and increase the effective degradation for the colony. Simulating smaller and more sparse trap sizes recovered antiphase behavior for neighboring biopixels (Suppl. Fig. 10). We also simulated the arrays with traps of two different sizes in different rows and recovered the experimental 2:1 biopixel resonance or 2:1 + antiphase behavior depending on the trap spacing (Fig. 3d, bottom).

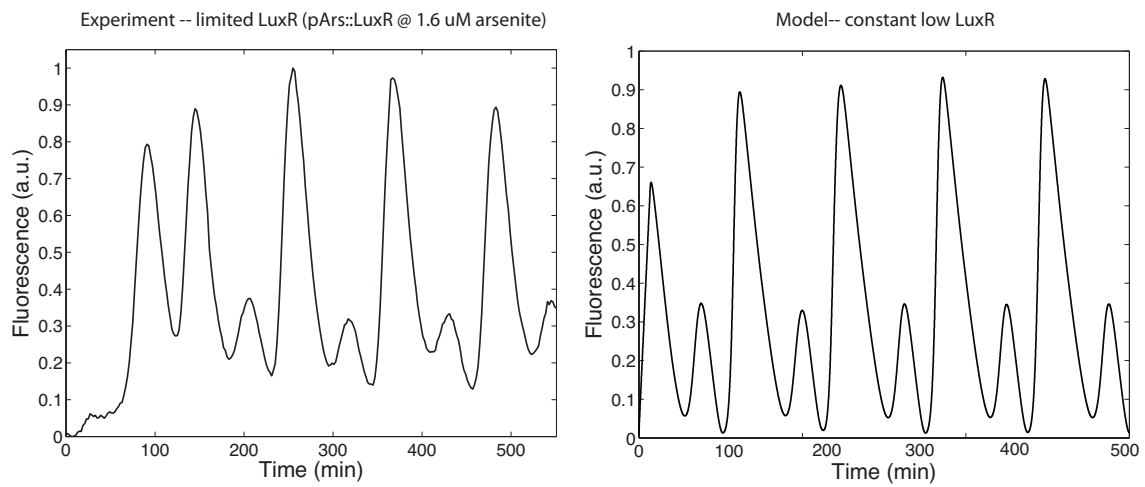


Supplementary Figure 10: Computational results depicting biopixel synchronicity as a function of trap separation distance. As biopixels are moved farther apart, the entropy increases due to decreased effective migration of H_2O_2 between colonies.

The model was also able to capture the alternating large and small amplitude oscillations observed in the ON/OFF biosensor (Suppl. Fig. 11). This behavior was seen when C_0 was increased 2-fold, capturing the decreased level of LuxR in ON/OFF experiments where it was the limiting factor for oscillations.



Supplementary Figure 11: Antiphase behavior of 4 neighboring biopixels having equal trap sizes and spacing $\Delta = 3$.



Supplementary Figure 12: Oscillations of alternating large and small amplitude when LuxR is limited in experiments and simulations. The alternating oscillations vanish when LuxR is restored to its normal level in the model. Experimentally, we were unable to build a system in which LuxR is tunable between big/small and normal amplitude regimes. This is probably due to the small dynamic range of arsenite promoter-driven output of LuxR compared to the level produced by 3 constitutively expressed copies in the original circuit.

References

- [1] Danino, T., Mondragon-Palomino, O., Tsimring, L. & Hasty, J. A synchronized quorum of genetic clocks. *Nature* **463**, 326–330 (2010).
- [2] Pedelacq, J.-D., Cabantous, S., Tran, T., Terwilliger, T. C. & Waldo, G. S. Engineering and characterization of a superfolder green fluorescent protein. *Nature Biotechnology* **24**, 79–88 (2006).
- [3] Stocker, J. *et al.* Development of a set of simple bacterial biosensors for quantitative and rapid measurements of arsenite and arsenate in potable water. *Environ. Sci. Technol* **37**, 4743–4750 (2003).
- [4] Keiler, K., Waller, P. & Sauer, R. Role of a peptide tagging system in degradation of proteins synthesized from damaged messenger rna. *Science* **271**, 990 (1996).
- [5] Quan, J. & Tian, J. Circular polymerase extension cloning of complex gene libraries and pathways. *PloS one* **4**, e6441 (2009).
- [6] Mather, W., Bennett, M., Hasty, J. & Tsimring, L. Delay-induced degrade-and-fire oscillations in small genetic circuits. *Physical Review Letters* **102**, 068105 (2009).

Supplementary Movies

Supplementary Movie 1. Timelapse fluorescence microscopy of a 200 trap sensor array displaying NDH-2 engineered synchronization. An EMCCD camera was used to keep exposure times extremely low (4X magnification, 20ms, 95% attenuation) to ensure no fluorescence interaction, hence the appearance of lower signal.

Supplementary Movie 2. Timelapse fluorescence microscopy of the 500 trap biosensor array showing the onset of synchronization from disparate initial conditions using period modulator circuit. Flashes indicate changes in arsenite concentration which result in changes in the oscillatory period.

Supplementary Movie 3. Timelapse fluorescence microscopy of a sensor array containing thresholding circuit. Red color indicates addition of $0.25 \mu\text{M}$ arsenite that initiates oscillations in blue.

Supplementary Movie 4. Timelapse fluorescence microscopy of a modified 500 trap sensor array in which traps are farther apart. This increased separation results in anti phase oscillations, where a biopixel and its nearest neighbors alternate bursts.

Supplementary Movie 5. Timelapse fluorescence microscopy of the 12,000 trap scaled up array showing oscillation and synchronization maintained over a maximum distance of 27 mm.

Supplementary Movie 6. Real time microscopy depicting the loading of our microfluidic device. Cells flow in from the cell port and fill the trapping regions.

Supplementary Movie 7. Timelapse fluorescence microscopy of a modified 500 trap sensor array in which traps of 2 sizes are present. This results in 2:1 resonant oscillations where larger traps oscillate at twice the frequency of smaller traps.

Supplementary Movie 8. Timelapse fluorescence microscopy of a 500 trap sensor array showing unsynchronized oscillations when NDH-2 is not present and high-intensity fluorescence bursts are not used.